Long-term continuous automatic modal tracking algorithm based on Bayesian inference

Siyuan Sun[1] , **Bin Yang**[1], **Qilin Zhang**[1], **Roland Wüchner**[2],
Licheng Pan[1] **and Haitao Zhu**[1]

Abstract
Modal tracking plays a vital role in structural health monitoring since changes in modal parameters help us understand a structure's dynamic characteristics and may reflect the potential deterioration of structural performance. Although numerous modal parameter estimation (MPE) methods exist, it is not guaranteed that an MPE process will exclude all spurious modes and not lose any physical modes every time over a long-term monitoring period. Relatively large damping of a structure, poor data quality, and significant changes in structural modal parameters may make the estimated modal parameters spurious, missing, or misclassified. It makes long-term modal tracking semiautomated or manual, which constrains timely downstream applications such as anomaly detection, condition assessment, and decision making. This research aims to propose a long-term continuous automatic modal tracking algorithm based on Bayesian inference even when the modal parameters, damping, and data quality change significantly. Bayesian inference is used to determine the physical modes from the results of existing MPE methods. Both the modes identified from the most recent response set and the modal probability model from multiple previous response sets are considered in the Bayesian model to better determine the physical modes from the results of MPE. Moreover, the proposed algorithm requires only three extra hyperparameters compared to general modal tracking algorithms, and they can be quickly determined by a grid search method. The performance of the proposed algorithm is verified by a numerical example and a real-world civil structure Z24 Bridge benchmark.

Keywords
Modal parameter estimation, modal tracking, Bayesian inference, structural health monitoring, automatization

Introduction

Recently, numerous vibration-based structural health monitoring (SHM) methods[1–6] have been developed for anomaly detection, condition assessment, and decision making. Among the various vibration properties, modal parameters such as frequencies and mode shapes provide vital information for understanding the characteristics of a structure[7] and are most widely used.[8] However, a significant downside of the modal extraction process is that it usually involves a substantial amount of user interaction, introducing a high level of uncertainty into the results.[9] Because long-term continuous modal tracking is critical for timely downstream applications, there is great interest in automating this process.

Modal tracking includes five stages: data collection, signal processing, system identification, determination of a validated set of modal parameters,[10] and physical mode selection. The last two stages require significant manual participation and are usually the most time-consuming stages, especially when selecting a mode through a stabilization diagram.[11] Numerous modal parameter estimation (MPE) methods have been developed to automate the fourth stage. These methods typically use specific clustering methods to determine the validated modal parameters. Magalhães et al.[12] implemented automatic modal identification using hierarchical clustering of candidate modes obtained through

[1]College of Civil Engineering, Tongji University, Shanghai, China
[2]TUM School of Engineering and Design, Technical University of Munich, München, Germany

Corresponding author:
Qilin Zhang, College of Civil Engineering, Tongji University, 1239 Siping Road, Shanghai 200092, China.
Email: zhangqilin@tongji.edu.cn

stochastic subspace identification driven by covariance (SSI-COV). Rainieri and Fabbrocino[5] used k-means clustering and statistical-threshold hierarchical clustering to filter candidate modes. Cardoso et al.[4] performed a second clustering after hierarchical clustering to circumvent the detection of spurious modes or the loss of physical modes. Some automatic MPE methods add an additional step before clustering to eliminate spurious or noise modes. Reynders et al.[10] removed spurious modes from the stabilization diagram using as many relevant single-mode validation criteria as possible. Ubertini et al.[6] eliminated noise modes through similarity checking on frequencies, damping ratios, and mode shapes. Neu et al.[3] used hard validation criteria and a k-means clustering approach to remove spurious modes. Charbonnel[1] partitioned candidate modes into spurious modes and potential physical modes using fuzzy c-means clustering. Tronci et al.[9,13] integrated the advantages of the above algorithms, presenting a multistage strategy where unsupervised tools and three clustering options are offered to a user to reach a reliable estimation of the modal parameters. In additon to clustering-based methods, some Bayesian modal identification methods[7,14–19] have boomed in recent years. They model the modal properties as random variables with a probability distribution that depends on the available information. The peak location of the distribution represents the posterior most probable values of the modal properties, which are considered to be the ones closest to the actual modal parameters. (In this sense, the derived parameters are no longer called estimates. However, for the convenience of expression, Bayesian modal identification method is still called a class of MPE methods hereinafter.) The covariance matrix of the modal properties implied by the distribution, that is, posterior covariance matrix, quantifies their identification uncertainty, which promotes to determine whether the identified parameters should be tracked.

Despite the continuous development of MPE research, it is not guaranteed that an MPE process will exclude all spurious modes and not lose any physical modes every time in long-term automatic continuous monitoring. Monitoring conditions (such as data quality), damping of the structure, and other factors will affect MPE results.[20] In addition, significant variations of modes[21–25] themselves make it difficult to determine whether they are physical modes. Suppose the MPE results are directly used for modal tracking; in that case, they may lead to the appearance of spurious modes, the absence of physical modes, or mode misclassification, which may distort the variation characteristic of the modes. The above issues directly or indirectly challenge automatic modal tracking and

mode-based structural assessment.[26] Recently, researchers have used prior reference modes to automatically select the physical modes from MPE. Cabboi et al.[27] used a clustering algorithm with low computational requirements to automatically analyze a stabilization diagram. Then, an algorithm takes the modes identified from the most recent response set as the reference modes to select the modes of the current response sets. Mao et al.[28] determined and updated the reference modes based on modes identified from multiple previous response sets. A Gaussian mixture model was used to perform modal tracking. Ubertini et al.[2] tracked the modes of a monumental masonry bell tower using the algorithm in research.[6] Tronci et al.[29] tracked the dynamic characteristics of the concrete-masonry Civic Tower in Rieti (Italy) equipped with a passive vibration control system, a nonconventional tuned mass damper, using a semiautomated identification procedure.[30] Yang et al.[26] proposed a multistage mode-tracking technique based on subspace correlation, a technique that updates the list of reference modes to include new modes.

However, among the above methods, a strategy that takes the modes identified from the most recent response set as the reference modes may be interfered with by certain spurious modes that are not successfully eliminated. A strategy that takes modes identified from multiple previous response sets as the reference modes may not adequately track the relatively fast-varying modal parameters. They work well when the data are of high quality, the damping of the structure is low (few spurious modes exist), and the variation in modal parameters is not obvious but may work poorly in the opposite situation. Our work aims to achieve long-term continuous and automatic modal identification even when the modal parameters and data quality change significantly. Bayesian inference is used to determine the physical modes from the results of existing MPE methods. Our algorithm combines the advantages of the above two strategies. Modes identified from the most recent response set and a modal probability model from multiple previous response sets were considered in the Bayesian inference model. These two considerations interact to help better select the physical modes from MPE. In addition, the proposed algorithm requires only three additional hyperparameters. They can be quickly determined through parameter determination methods such as grid search.

This algorithm can be used after any MPE method. Although there are numerous system identification algorithms, this study uses SSI-COV as the system identification algorithm in MPE. The following Section "Research basis and problem description" presents the basics of SSI-COV and automatic MPE. Some

examples are given to illustrate how the problems resulting from MPE affect modal tracking. In Section "Long-term continuous automatic modal tracking algorithm based on Bayesian inference," the algorithm based on Bayesian inference is presented. In Section "Numerical example," a numerical example is used to verify the algorithm's performance, and a simple modal tracking algorithm is employed for comparison purposes. Section "Empirical studies" reports the results of an experiment in which the proposed algorithm and the simple tracking algorithm are applied to a real-world structure Z24 bridge benchmark. Finally, the last section concludes the paper.

Research basis and problem description

For a complete introduction to the stochastic subspace identification theory, please refer to research.[31] Briefly, the basic model for SSI-COV can be expressed as a classical state-space form of the discrete-time equation of motion for a linear, time-invariant n-DOF system under the assumption of white noise excitation:

$$\begin{cases} x_{k+1} = Ax_k + w_k, \\ y_k = Cx_k + v_k. \end{cases} \tag{1}$$

where x_k is the $n \times 1$ discrete-time state vector at time k; y_k is the measurement output vector of $l \times 1$ at time k; l is the number of sensors; A is an $n \times n$ discrete-state matrix; C is an $l \times n$ discrete output matrix; and w_k and v_k represent the effects of unknown inputs, that is, modeling inaccuracies and measurement noise, respectively. The vectors are assumed to be zero-mean implementations of stationary stochastic processes and are independent of the actual state.

Given these assumptions, the modal parameters can be extracted using only the output response.[31] Ideally, the number of modes identified equals the model order, which matches the rank r of the Toeplitz matrix (containing the covariance functions of the dynamic response). Therefore, a reasonable estimate of the model order could come from finding a gap between two consecutive singular values of the Toeplitz matrix.[27] However, due to model error, measurement inaccuracy, and covariance estimation accuracy in data processing, in practice this method has not proven effective. A possible way to overcome this is to set the rank r of the Toeplitz matrix within a defined N_{min}–N_{max} interval. The values of the physical modes are close at different rank r. The spurious modes are discrete at different rank r because of their instability. Based on this principle, a so-called stabilization diagram[31] (Figure 6) is then used to help determine these physical modes. In a stabilization diagram, the modal parameter estimates at different rank r are represented together (x-axis – natural frequency of the mode estimates; y-axis – order of the model, i.e., rank r). Modes that appear with consistent frequency, mode shape, and damping are classified as stable and are likely to be physical. Modes that only appear sporadically are considered spurious.

The stabilization diagram alone does not solve the problem of modal parameter identification. Rather, it serves as a graphical tool to aid in the manual selection of modes that are more likely to represent physical modes. To reduce the need for user involvement, clustering algorithms are employed to automatically analyze the stabilization diagram. These algorithms typically involve two main steps: (1) clustering poles with consistent parameters, and (2) selecting representative quantities for clusters as the modal parameters of physical modes. However, challenges still exist. For instance, to identify weakly excited modes (red box in Figure 6), one may need to set a relatively large value for N_{max} to include sufficient information. However, a large N_{max} also increases computational time, and the presence of non-physical poles (green box in Figure 6), making it difficult to distinguish between physical and spurious poles.[27] Since automatic methods generally aim to identify vertical alignments of the stabilization diagram by clustering poles with consistent parameters, they may output multiple similar modes which are supposed to be spurious modes. In Figure 6, for example, the identified modal frequencies by a hierarchical clustering algorithm[12] are (1.107, 1.108, 3.906, 4.418, 4.467, 4.509, 4.513, 8.587, 8.594, 8.737, 10.298, 15.229, 15.530, 15.568, 18.338, 18.502, 18.509, 18.533, 18.540, 18.686), while the analytical frequencies are (1.111, 3.914, 4.510, 8.755, 10.290, 15.267, 18.345, 18.538) (Figure 6).

During the long-term modal tracking process, it is likely that physical modes may not be identified and spurious modes may also occur simultaneously. Worse still, when the modal parameters change significantly, it becomes more challenging to determine whether a mode estimated from MPE is a physical mode and correctly classify the physical modes. Methods using the last successfully tracked mode as a reference mode can track such changes, but also be susceptible to spurious modes, risking tracking failure. A probabilistic model of past modal parameters can avoid this issue, but when modes change significantly, the new results from MPE may exceed the probability threshold, which also results in tracking failure. Therefore, it is necessary to develop a robust long-term continuous automatic modal tracking algorithm to effectively select the
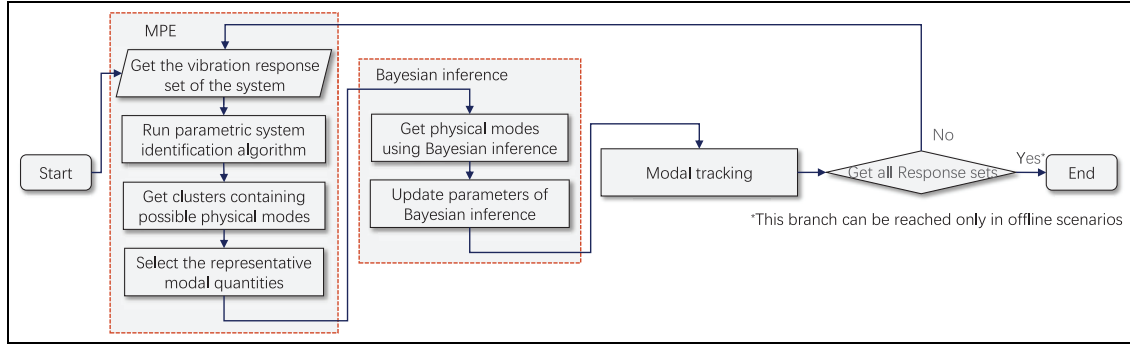
Figure 1. Complete flow chart of the long-term continuous automatic modal tracking algorithm.

physical modes from the MPE results when faced with various complicated situations.

Long-term continuous automatic modal tracking algorithm based on Bayesian inference

The complete flow chart of the long-term continuous automatic modal tracking algorithm is shown in Figure 1. As research on MPE is relatively mature, this study does not focus on MPE research but adopts an existing automatic MPE algorithm. The Bayesian inference process is performed after the MPE process. The inference process can be divided into two steps: (1) obtaining the physical modes, which will be presented in Section "Obtain physical modes using Bayesian inference" and (2) updating the inference parameters, which will be presented in Section "Update Bayesian inference parameters." Section "Hyperparameters for Bayesian inference and some details" describes the selection of the hyperparameters for Bayesian inference and algorithm details. Section " Advantages of the proposed algorithm" discusses the algorithm's advantages.

Obtain physical modes using Bayesian inference

The proposed algorithm is based on a probability model. As mentioned in the previous section, the probability model is less susceptible to spurious modes, but it performs poorly when modal parameters change significantly. To address this issue, this algorithm uses the last successfully identified modal parameters as prior knowledge for the Bayesian model to modify the probability density, which can both avoid interference from spurious modes and track significantly changing modes.

The Bayesian inference form is:

$$p\left(\boldsymbol{\theta}_k^j \middle| \mathcal{R}_j\right) = \frac{p\left(\boldsymbol{\theta}_k^j\right)p\left(\mathcal{R}_j \middle| \boldsymbol{\theta}_k^j\right)}{p\left(\mathcal{R}_j\right)} \qquad (2)$$

Parameter $\boldsymbol{\theta}_k^j$ represents the k-th set of modal parameters from MPE corresponding to physical mode j. Here, the modal parameters refer to the composition of the natural frequency and mode shape. Because the values in the mode shape vector only represent relative magnitudes, and considering making the values in the mode shape vector similar in size to the frequency, the values of the mode shape vector are determined by their root mean square being equal to the corresponding frequency value. When the number of channels is large, the root mean square of the mode shape vector can be appropriately amplified. Modal damping is not included because it is related to the energy of the vibration[12] and has a large dispersion,[16] which may interfere with the identification. $\mathcal{R}_j$ represents the reference modal parameters of physical mode j. $\mathcal{R}_j$ is also composed of the natural frequency and mode shape and therefore is an $(l + 1) \times 1$ vector. The value of $\mathcal{R}_j$ will be discussed in Section "Update Bayesian inference parameters." Parameter $k = 1, 2, …, N_c$ where N_c is the number of modes from MPE. N_c is a variable that depends on the MPE results. Parameter $j = 1, 2,…, N_r$ where N_r is the number of reference modes. It is a hyperparameter specified according to knowledge of the structure. The value of N_r will be discussed in Section "Hyperparameters for Bayesian inference and some details."

$p\left(\boldsymbol{\theta}_k^j \middle| \mathcal{R}_j\right)$ is the probability density at which the k-th set of modal parameters from MPE corresponds to physical mode j under the condition that the reference modal parameters of physical mode j are $\mathcal{R}_j$. On the right side of Equation (2), $p\left(\boldsymbol{\theta}_k^j\right)$ is the probability density at which the k-th set of modal parameters from MPE corresponds to physical mode j. Assume that the modal parameters of physical mode j follow a multivariate Gaussian distribution $N_{l+1}(\boldsymbol{\mu}_j, \boldsymbol{\Sigma}_j)$, then,

$$p(\boldsymbol{\theta}_k^j) = \frac{1}{\sqrt{(2\pi)^{l+1}|\boldsymbol{\Sigma}_j|}} \exp\left(-\frac{1}{2}(\boldsymbol{\theta}_k - \boldsymbol{\mu}_j)^T \boldsymbol{\Sigma}_j^{-1}(\boldsymbol{\theta}_k - \boldsymbol{\mu}_j)\right)$$

$$(3)$$

where $\boldsymbol{\theta}_k$ is the k-th set of modal parameters from MPE. Parameter $\boldsymbol{\mu}_j$ is an $(l + 1) \times 1$ mean vector of the multivariate Gaussian distribution of physical mode j. Parameter $\boldsymbol{\Sigma}_j$ is an $(l + 1) \times (l + 1)$ covariance matrix. Their calculations are discussed in Section "Update Bayesian inference parameters."

$p(\mathcal{R}_j | \boldsymbol{\theta}_k^j)$ is the probability density at which the reference modal parameters of physical mode j is $\mathcal{R}_j$ under the condition that the k-th set of modal parameters from MPE corresponds to physical mode j. $\mathcal{R}_j$ also follows a multivariate Gaussian distribution $N_{l+1}(\boldsymbol{\mu}_j, \boldsymbol{\Sigma}_j)$ since it is a reference to physical mode j. When the modal parameters of physical mode j is θ_k, the Gaussian distribution changes from $N_{l+1}(\boldsymbol{\mu}_j, \boldsymbol{\Sigma}_j)$ to $N_{l+1}(\boldsymbol{\theta}_k, \boldsymbol{\Sigma}_j)$. $\boldsymbol{\Sigma}_j$ stays the same because only the values of the physical modal parameters change, but their fluctuations do not change. Therefore,

$$p(\mathcal{R}_j | \boldsymbol{\theta}_k^j) = \frac{1}{\sqrt{(2\pi)^{l+1}|\boldsymbol{\Sigma}_j|}}$$
$$\exp\left(-\frac{1}{2}(\mathcal{R}_j - \boldsymbol{\theta}_k)^T \boldsymbol{\Sigma}_j^{-1}(\mathcal{R}_j - \boldsymbol{\theta}_k)\right)$$

$$(4)$$

$p(\mathcal{R}_j)$ is the probability density at which the reference modal parameters of physical mode j are $\mathcal{R}_j$. As mentioned above, $\mathcal{R}_j$ follows a multivariate Gaussian distribution $N_{l+1}(\boldsymbol{\mu}_j, \boldsymbol{\Sigma}_j)$. Hence,

$$p(\mathcal{R}_j) = \frac{1}{\sqrt{(2\pi)^{l+1}|\boldsymbol{\Sigma}_j|}} \exp\left(-\frac{1}{2}(\mathcal{R}_j - \boldsymbol{\mu}_j)^T \boldsymbol{\Sigma}_j^{-1}(\mathcal{R}_j - \boldsymbol{\mu}_j)\right)$$

$$(5)$$

By traversing all k and j in Equation (2), a posteriori probability density matrix is obtained:

$$\boldsymbol{P}_{N_r \times N_c} = \begin{bmatrix} p(\boldsymbol{\theta}_1^1|\mathcal{R}_1) & p(\boldsymbol{\theta}_2^1|\mathcal{R}_1) & \cdots & p(\boldsymbol{\theta}_{N_c}^1|\mathcal{R}_1) \\ p(\boldsymbol{\theta}_1^2|\mathcal{R}_2) & p(\boldsymbol{\theta}_2^2|\mathcal{R}_2) & \cdots & p(\boldsymbol{\theta}_{N_c}^2|\mathcal{R}_2) \\ \vdots & \vdots & \ddots & \vdots \\ p(\boldsymbol{\theta}_1^{N_r}|\mathcal{R}_{N_r}) & p(\boldsymbol{\theta}_2^{N_r}|\mathcal{R}_{N_r}) & \cdots & p(\boldsymbol{\theta}_{N_c}^{N_r}|\mathcal{R}_{N_r}) \end{bmatrix}$$

$$(6)$$

The mode from MPE that best matches each physical mode can be determined by maximizing each row of the probability density matrix:

$$\boldsymbol{p}_{\max} = \begin{bmatrix} p_{\max 1}, \text{ind}1 \\ p_{\max 2}, \text{ind}2 \\ \vdots \\ p_{\max N_r}, \text{ind}N_r \end{bmatrix}$$

$$= \begin{bmatrix} \max\left(p(\boldsymbol{\theta}_1^1|\mathcal{R}_1), p(\boldsymbol{\theta}_2^1|\mathcal{R}_1), \cdots, p(\boldsymbol{\theta}_{N_c}^1|\mathcal{R}_1)\right) \\ \max\left(p(\boldsymbol{\theta}_1^2|\mathcal{R}_2), p(\boldsymbol{\theta}_2^2|\mathcal{R}_2), \cdots, p(\boldsymbol{\theta}_{N_c}^2|\mathcal{R}_2)\right) \\ \vdots \\ \max\left(p(\boldsymbol{\theta}_1^{N_r}|\mathcal{R}_{N_r}), p(\boldsymbol{\theta}_2^{N_r}|\mathcal{R}_{N_r}), \cdots, p(\boldsymbol{\theta}_{N_c}^{N_r}|\mathcal{R}_{N_r})\right) \end{bmatrix}$$

$$(7)$$

where $p_{\max j}$ and $\text{ind}j$ are the maximum value and its index of $[p(\boldsymbol{\theta}_1^j|\mathcal{R}_j), p(\boldsymbol{\theta}_2^j|\mathcal{R}_j), \cdots, p(\boldsymbol{\theta}_{N_c}^j|\mathcal{R}_j)]$. By comparing each $p_{\max j}$ with the threshold of probability density $p_{\text{threshold}j}$, we can decide whether to accept the mode from MPE:

$$\boldsymbol{\theta}_{\text{physical}j} = \boldsymbol{\theta}_{\text{ind}j}, \quad p_{\max j} > p_{\text{threshold}j} \tag{8}$$

where $\boldsymbol{\theta}_{\text{physical}j}$ are the selected modal parameters of physical mode j. $\boldsymbol{\theta}_{\text{ind}j}$ is the $\text{ind}j$−th mode from MPE. The greater the value of $p_{\max j}$ is, the more likely $\boldsymbol{\theta}_{\text{ind}j}$ is to be a physical mode j, and vice versa.

Update Bayesian inference parameters

After modal tracking of the current response set, it is necessary to update the Bayesian inference parameters for modal tracking of the subsequent response set. The parameters to be updated are $\mathcal{R}_j$, $p_{\text{threshold}j}$, $\boldsymbol{\mu}_j$, and $\boldsymbol{\Sigma}_j$, where all of them can be updated automatically.

For $\mathcal{R}_j$, if $p_{\max j}$ is more than $p_{\text{threshold}j}$, it will be updated to the combination of mode shape and frequency of identified physical mode j from the current response set, which is $\boldsymbol{\theta}_{\text{physical}j}$. However, if $p_{\max j}$ is less than or equal to $p_{\text{threshold}j}$, it indicates that the current response set does not contain any identified mode for mode j, and $\mathcal{R}_j$ will be retained for the next set. If this situation occurs repeatedly, it may imply a persistent abnormal change in mode j. In such cases, it is recommended to investigate the underlying cause and consider manual intervention if necessary.

The probability density threshold for mode j ($p_{\text{threshold}j}$) is set to the probability density corresponding to the percentile (e.g., 95%) of the Gaussian distribution $N_{l+1}(\boldsymbol{\mu}_j, \boldsymbol{\Sigma}_j)$ mentioned in the previous section. This value is equivalent to the probability density of any point on the surface of a hyperellipsoid with $l + 1$ dimensions (Figure 2 schematically shows this with 2-d Gaussian distribution). To represent this hyperellipsoid, we can define a variable z as $z = (\boldsymbol{x} - \boldsymbol{\mu}_j)^T \boldsymbol{\Sigma}_j^{-1}(\boldsymbol{x} - \boldsymbol{\mu}_j)$. Since $\boldsymbol{x} \sim N_{l+1}(\boldsymbol{\mu}_j, \boldsymbol{\Sigma}_j)$, we have $z \sim \chi_{l+1}^2$,
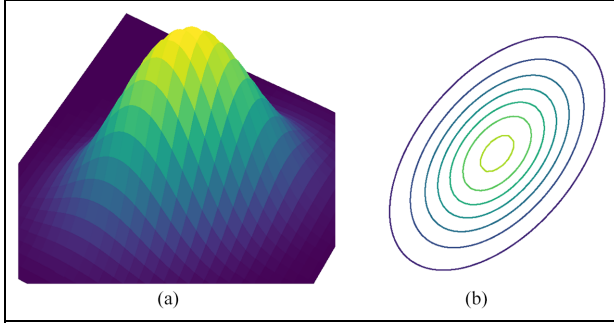
Figure 2. (a) 2-d Gaussian distribution, and (b) equiprobable density line.

where χ^2 represents the chi-squared distribution.[32] Therefore, the problem can be equivalent to finding a value c in the z space such that $P(z \leqslant c) = 0.95$. Since $z \sim \chi^2_{l+1}$, c is exactly the 0.95 quantile of χ^2_{l+1}, that is, the hyperellipsoid can be expressed as $(x - \mu_j)^T \Sigma_j^{-1}(x - \mu_j) \leqslant c$. The threshold $p_{\text{threshold}j}$ can be obtained by:

$$p_{\text{threshold}j} = p_p = p\left(\mu_j + \text{ev}(\Sigma_j)\sqrt{\text{ew}(\Sigma_j) \times c}\right) \quad (9)$$

where p is the probability density function of the Gaussian distribution $N_{l+1}(\mu_j, \Sigma_j)$; p_p is the probability density of any point on the hyperellipsoid surface; μ_j denotes the coordinates of the center of the hyperellipsoid; $\text{ev}(\Sigma_j)$ represents any eigenvector of Σ_j, and also the direction of the axis of the hyperellipsoid; $\text{ew}(\Sigma_j)$ is the corresponding eigenvalue of Σ_j; $\sqrt{\text{ew}(\Sigma_j) \times c}$ represents the semi-length of that axis. Equation (9) represents the probability density of the intersection points between any principal axis of the hyperellipsoid and the hyperellipsoid surface for the Gaussian distribution $N_{l+1}(\mu_j, \Sigma_j)$, which is also the $p_{\text{threshold}j}$ we are seeking.

It cannot be guaranteed that when $p_{\text{max}j}$ is larger than $p_{\text{threshold}j}$, $\theta_{\text{ind}j}$ must correspond to physical mode j (Equation (8)). A larger $p_{\text{threshold}j}$ leads to more accurate tracking but also reduces the number of modes that should be tracked. A smaller $p_{\text{threshold}j}$ can track more modes but may cause spurious modes to appear. Thus, the determination of $p_{\text{threshold}j}$ is heuristic.

Parameters μ_j and Σ_j are the mean vector and covariance matrix of the multivariate Gaussian distribution of the modal parameters of physical mode j, respectively. They can be obtained from predefined m-set physical modal parameters successfully identified from the past response sets:

$$\mu_j = \text{mean}\left(\theta_{\text{physical}j,1}, \theta_{\text{physical}j,2} \ldots \theta_{\text{physical}j,m}\right) \quad (10)$$

$$\Sigma_j = \text{cov}\left(\theta_{\text{physical}j,1}, \theta_{\text{physical}j,2} \ldots \theta_{\text{physical}j,m}\right) \quad (11)$$

where $\theta_{\text{physical}j,p}$ is the modal parameters of physical mode j successfully identified from the last p-th response set. However, the position of one sensor may result in very small value for an individual element of the mode shape, causing Σ_j obtained from Equation (11) to have very a small eigenvalue. This can cause one of the ellipsoidal axes of the Gaussian model to be very short, greatly reducing the robustness of the algorithm. Therefore, Σ_j is modified as follows:

$$\begin{cases} \Sigma_j = Q^T Q \\ \Lambda[k,k] = \max\left([k,k], \lambda_{\min_j}\right) \end{cases} \quad (12)$$

where Λ and Q are the diagonal eigenvalue matrix and eigenvectors, respectively. $\Lambda[k,k] = \max(\Lambda[k,k], \lambda_{\min})$ in Equation (12) is equivalent to relaxing the constraints on extremely small elements in the mode shape. If $\lambda_{\min_j}$ is set to zero, this implies that no alterations are made to Σj. In practical applications, it is recommended that $\lambda_{\min_j}$ be set to 0.1 times the frequency of mode j. On the one hand, these extremely small eigenvalues cannot serve as one of the structural features, so they can be appropriately relaxed. On the other hand, it is also necessary to relax these constraints because it can greatly improve the robustness of the algorithm.

Hyperparameters for Bayesian inference and some details

There are several hyperparameters for Bayesian inference in this algorithm. They are the percentile of the Gaussian distribution, the allowed minimum eigenvalue $\lambda_{\min_j}$ of Σ_j, the number m of last successfully identified response sets to update μ_j and Σ_j, the initial values of $\mathcal{R}_j$, μ_j, and Σ_j. In general, setting the first two hyperparameters to 95% and 0.1 times the frequency of mode j, respectively, can work well for most cases. The choice of m does not significantly affect the results of the algorithm and can typically be set to 50. If necessary, these hyperparameters can also be quickly determined by using a grid search method. The initial values of $\mathcal{R}_j$, μ_j, and Σ_j can be obtained by first clustering the first several response sets, then selecting the clusters that represent the physical modes. In addition, any other knowledge of the structural can also be used to help determine these initial values.

The pseudocode of the algorithm is shown as Algorithm 1. H_μ is an $N_r \times (l+1) \times m$ three-dimensional array. It is used to store identified θ_{physical} from each response set. The count in the pseudocode is used for removing outdated modes in H_μ and H_Σ. There is no unique strategy for removing outdated modes, and other reasonable strategies are acceptable. $H_\mu(j)$ is an $(l+1) \times m$ two-dimensional subarray of H_μ to store

Algorithm 1. Long-term continuous automatic modal tracking algorithm based on Bayesian inference.

Input: m, initial $\mathcal{R}_j$, $\boldsymbol{\mu}_j$, and $\boldsymbol{\Sigma}_j$
Output: $\boldsymbol{\theta}_{\mathrm{physical}j}$

1   **Initialize** $H_{\boldsymbol{\mu}}$, $H_{\boldsymbol{\Sigma}}$, $count = 0$ // $H_{\boldsymbol{\mu}}$, $H_{\boldsymbol{\Sigma}}$ are used to store the identified $\boldsymbol{\theta}_{\mathrm{physical}j}$ to estimate the $\boldsymbol{\mu}_j$ and $\boldsymbol{\Sigma}_j$

2   **while** MPE results $\boldsymbol{\theta}_{1,2\ldots N_c}$ arrive **do**

3       $count = count + 1$

4   // Form a posterior probability density matrix

5   **for** *each* $j(1 \leq j \leq N_r)$ **do**

6   **for** *each* $k(1 \leq k \leq N_c)$ **do**

7              $\boldsymbol{\theta}_k = \mathrm{normalize}(\boldsymbol{\theta}_k, \mathcal{R}_j)$

8              $\boldsymbol{P}_{N_r \times N_c}[j, k] = p(\mathcal{R}_j | \boldsymbol{\theta}_k^j) p(\boldsymbol{\theta}_k^j) / p(\mathcal{R}_j)$

9   // Obtain $\boldsymbol{\theta}_{\mathrm{physical}j}$ and update data

10   **for** *each* $j(1 \leq j \leq N_r)$ **do**

11          $[p_{\mathrm{max}j}, \mathrm{ind}j] = \max(\boldsymbol{P}_{N_r \times N_c}[j,:])$

12          $\boldsymbol{\theta}_{\mathrm{ind}j} = \mathrm{normalize}(\boldsymbol{\theta}_{\mathrm{ind}j}, \mathcal{R}_j)$

13   get $p_{\mathrm{threshold}j}$ from Equation 9

14   **if** $p_{\mathrm{max}j} > p_{\mathrm{threshold}j}$ **then**

15              $\boldsymbol{\theta}_{\mathrm{physical}j} = \boldsymbol{\theta}_{\mathrm{ind}j}$

16              $H_{\boldsymbol{\mu}}.\mathrm{append}(\boldsymbol{\theta}_{\mathrm{physical}j})$, $H_{\boldsymbol{\Sigma}}.\mathrm{append}(\boldsymbol{\theta}_{\mathrm{physical}j})$

17   **while** $\mathrm{length}(H_{\boldsymbol{\mu}}) > m_{\boldsymbol{\mu}}$ *or* $count\%m_{\boldsymbol{\mu}} == 0$ **do** // % is a redundant symbol. This statement is used to delete early historical data that is no longer meaningful

18                  $H_{\boldsymbol{\mu}}.\mathrm{pop}(1)$

19   **while** $\mathrm{length}(H_{\boldsymbol{\Sigma}}) > m_{\boldsymbol{\Sigma}}$ *or* $count\%m_{\boldsymbol{\Sigma}} == 0$ **do** $H_{\boldsymbol{\Sigma}}.\mathrm{pop}(1)$

20   **else**

21              $\boldsymbol{\theta}_{\mathrm{spurious}j} = \boldsymbol{\theta}_{\mathrm{ind}j}$

22   **while** $count\%m_{\boldsymbol{\mu}} == 0$ **do** $H_{\boldsymbol{\mu}}.\mathrm{pop}(1)$

23   **while** $count\%m_{\boldsymbol{\Sigma}} == 0$ **do** $H_{\boldsymbol{\Sigma}}.\mathrm{pop}(1)$

24   // Parameters updating

25   **for** *each* $j(1 \leq j \leq N_r)$ **do**

26   **if** $\mathrm{length}(H_{\boldsymbol{\mu}}) == m$ **then**

27              $\boldsymbol{\mu}_j = \mathrm{mean}(H_{\boldsymbol{\mu}})$

28              $\boldsymbol{\Sigma}_j = \mathrm{cov}(H_{\boldsymbol{\Sigma}})$

29   modify $\boldsymbol{\Sigma}_j$ according Equation 12

---

identified $\boldsymbol{\theta}_{\mathrm{physical}j}$. When the number of stored $\boldsymbol{\theta}_{\mathrm{physical}j}$ equals m, parameter $\boldsymbol{\mu}_j$ will be updated.

Advantages of the proposed algorithm

Equation (2) considers the modes identified from the most recent response set ($\mathcal{R}_j$) as well as the modal probability model from multiple previous response sets ($N_{l+1}(\boldsymbol{\mu}_j, \boldsymbol{\Sigma}_j)$). This approach combines the benefits of both, allowing for the tracking of y changing modes while also being resistant to interference from spurious modes. For the sake of illustration, their advantages are discussed below using only the frequency component in $\boldsymbol{\theta}_k$, $\mathcal{R}_j$, $\boldsymbol{\mu}_j$, and $\boldsymbol{\Sigma}_j$ (i.e., θ_k, $\mathcal{R}_j$, μ_j and σ_j in this subsection).

Figure 3 shows four scenarios for frequency variation. A significant change in frequency (orange point) appears in Figure 3(a). If the probability density modified by Bayesian inference is higher than 95% percentile of the Gaussian distribution, it can be successfully tracked. In Figure 3(b), a frequency of similar magnitude reappears. Since the left orange dot has been taken as $\mathcal{R}_j$ in Equation (2), $\mathcal{R}_j$ makes it easier for the algorithm to identify the new frequency. Thus far, there is no significant difference between the proposed algorithm and other simpler tracking algorithms. However,
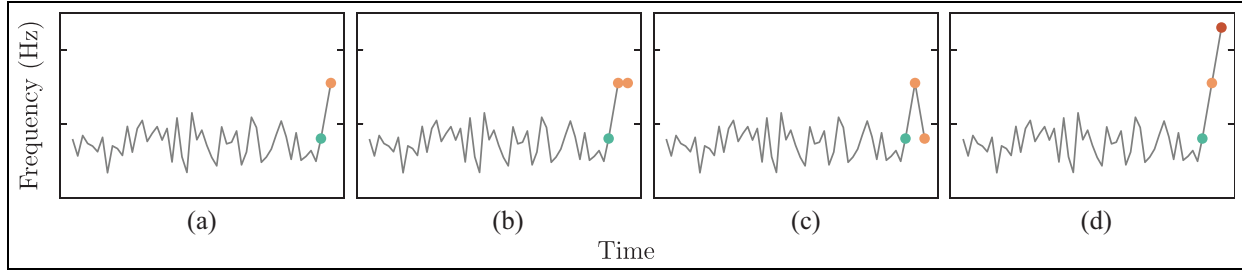
Figure 3. (a) The appearance of significant frequency change, (b) the same level of significant frequency change appeared again, (c) return to the original frequency level, and (d) more significant frequency changes appear.

if the new frequencies in Figure 3(c) and (d) appear simultaneously, it is difficult for reference-mode-based algorithms to determine which frequency is the physical frequency based on $\mathcal{R}_j$ alone because the distance between the new and previous frequencies is almost the same in both figures. Using our algorithm, the modal probability model $N(\mu_j, \sigma_j)$ specifies the level of the previous frequency. Therefore, the new frequency in Figure 3(c) is more likely to be chosen as the physical frequency. In terms of Figure 3(d), if the red dot should have been identified as the physical frequency, it changed quickly in a short period of time. In this situation, the strategy that only depends on the modal probability model may fail. With our algorithm, $\mathcal{R}_j$ indicates that an obviously changed orange dot has been identified. Therefore, the red dot is more likely to be accepted. It can be seen that the advantages of the two strategies $\left(\mathcal{R}_j \text{ and } N_{l+1}\left(\boldsymbol{\mu}_j, \boldsymbol{\Sigma}_j\right)\right)$ are combined by our algorithm. These two strategies interact to help better select the physical modes from MPE.

Numerical example

A numerical example is used to test the algorithm's performance. Section "Structure overview" first introduces the structure overview. Section "Numerical example setup" illustrates the setup of numerical example. The generation of response sets and MPE results is described in Section "Generation of response sets and MPE results." Section "Continuous modal tracking results" presents the results and comparison of continuous modal tracking using both a simple modal tracking algorithm and the proposed algorithm.

Structure overview

For simplicity and without loss of generality, a simply supported slab was used for the numerical example to verify the effectiveness of the proposed algorithm. Its length, width, and height are 15, 6, and 0.15 m, respectively. The material density is 2600 kg/m³, and the elastic modulus is 3.45×10^{10} Pa. The first eight modes are studied. The analytical natural frequencies and mode shapes of modes 1–8 are shown in Figure 4. The damping ratios of each mode are set to 1%.

Numerical example setup

A total of 300 synthetic datasets from three scenarios, were generated for the numerical example. In the first 100 datasets, the mass and stiffness of the structure remained constant. In the second 100 datasets, all masses underwent periodic changes to alter the frequencies and mode shapes of the structure. In the final 100 datasets, beyond the impacts of the second scenario, a progressive reduction of up to 50% in local stiffness was implemented on the structure to simulate localized damage. The abnormal area is indicated in Figure 5. Based on the above variation, Gaussian random variations were applied to the mass and stiffness to provide some randomness. The following equations provide detailed changes in mass and stiffness over datasets:

$$D_i(k) = D \times (1 + \Delta D_i(k)) \tag{13}$$

$$E_i(k) = E \times (1 + \Delta E_i(k)) \tag{14}$$

$$\Delta D_i(k) = \begin{cases} \text{GN}(\mu = 0, \sigma = 0.01), & 0 < k \leqslant 100, \\ \text{GN}(\mu = 0, \sigma = 0.01) + 0.03 \sin\left(2\pi \cdot 3 \cdot \frac{k-100}{100}\right), & k > 100, \end{cases} \tag{15}$$

$$\Delta E_i(k) = \begin{cases} \text{GN}(\mu = 0, \sigma = 0.02), & 0 < k \leqslant 200, \\ \text{GN}(\mu = 0, \sigma = 0.02), & k > 200, \text{normal area}, \\ \text{GN}(\mu = 0, \sigma = 0.02) - 0.5\frac{k-200}{100}, & k > 200, \text{abnormal area}. \end{cases} \tag{16}$$
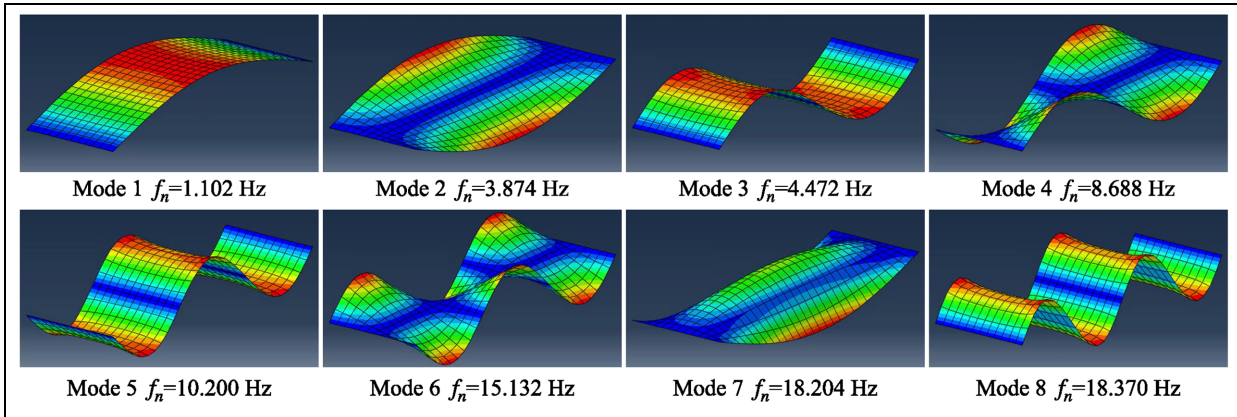
Figure 4. Analytical natural frequencies, and mode shapes of the numerical example.

where $k = 1, 2, ..., 300$ is the index of the datasets. $D_i(k)$ and $E_i(k)$ are the material density and elastic modulus, respectively. $\Delta D_i(k)$ and $\Delta E_i(k)$ are the change rates at index k relative to D and E, respectively. $GN(\mu, \sigma)$ represents a Gaussian number with mean μ and variance σ.

Generation of response sets and MPE results

A continuous Gaussian white noise excitation is applied to the structure. The structural response over 300 datasets at 100 Hz is calculated according to the excitation and parameters of the structure using the modal dynamics step of ABAQUS. The response within a 10-min time window is taken as a response set. The MPE method SSI-COV is then applied to each response set in turn. According to the discussion in Section "Research basis and problem description," the range of rank r of the Toeplitz matrix, that is, $N_{\min}$–$N_{\max}$, is set to 20–70 to identify weakly excited modes, such as mode 8 (Figure 4).

Continuous modal tracking results

The stabilization diagram of the first response set is shown in Figure 6. The Figure shows that the first four modes exhibit distinct vertical lines. However, the other modes are plagued by numerous spurious modes, which makes them challenging to track. Twenty modes are obtained by automatic MPE, and their frequencies are (1.107, 1.108, 3.906, 4.418, 4.467, 4.509, 4.513, 8.587, 8.594, 8.737, 10.298, 15.229, 15.530, 15.568, 18.338, 18.502, 18.509, 18.533, 18.540, 18.686). In fact, eight modes corresponding to frequencies (1.111, 3.914, 4.510, 8.755, 10.290, 15.267, 18.345, 18.538) should be identified as physical modes. (Note that since the Gaussian random numbers were added to the density and elastic modulus, the frequencies here are not
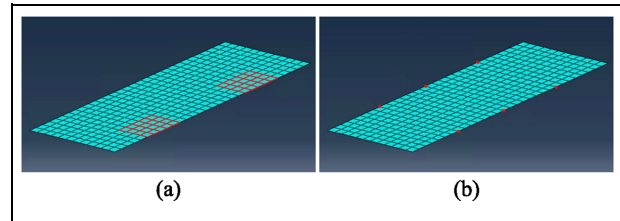

Figure 5. (a) The simulated abnormal area in the third scenario (highlighted in red), and (b) the sensor locations (marked by red dots).

identical to those depicted in Figure 4.) Suppose only the MPE method is applied iteratively for modal tracking on these response sets. In that case, as shown in Figure 7(a), modal tracking may not work well. In Figure 7(a), some spurious modes are shown. Moreover, which physical mode the modes obtained by MPE belong to cannot be automatically determined. The black lines in Figure 7 represent the frequencies of the analytical modes.

It is necessary to make modal tracking work well. To set proper hyperparameters, a hierarchical clustering algorithm[12] is applied to all the modes from the first 50 response sets, and finally 8 clusters representing physical modes are selected. $\mathcal{R}_j$ is taken from the representative modal quantities of cluster j. $\boldsymbol{\mu}_j$ and $\boldsymbol{\Sigma}_j$ are the mean vector and modified covariance matrix of cluster j, respectively. The value of m is set to 50. $p_{\text{threshold}j}$ takes the 95% percentile of the Gaussian distribution $N_9(\boldsymbol{\mu}_j, \boldsymbol{\Sigma}_j)$. And the allowed minimum eigenvalue $\lambda_{\min_j}$ of $\boldsymbol{\Sigma}_j$ is set to 0.1 times the frequency of mode j.

The results of the proposed modal tracking algorithm are presented in Figure 7(c), while a simple modal tracking algorithm based on reference modes is used for comparison, and its results are shown in Figure 7(b). For further details on the algorithm, please refer to the research paper.[33] Figure 7(b) and (c)
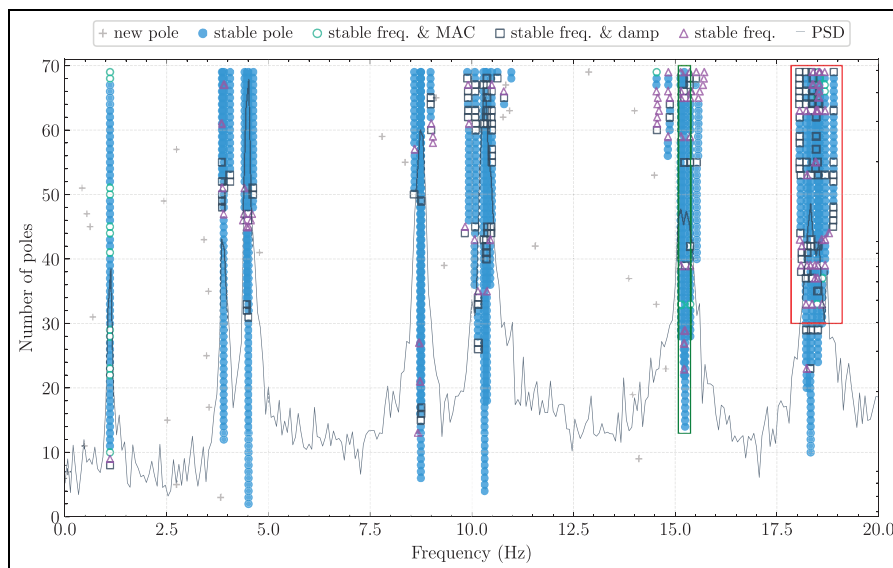
Figure 6. The stabilization diagram for the numerical example.

shows that both algorithms exhibit commendable performance for modes 2 through 7. However, the proposed algorithm outshines the simple modal tracking algorithm when it comes to modes 1 and 8. In the case of mode 1, for some datasets, modes that should have been identified as mode 1 by the simple modal tracking algorithm were overlooked. This oversight arises due to the little variation in frequency and mode shape values for mode 1 in this numerical example, thereby resulting in a small threshold associated with the standard deviation of historical modal parameters, as per Equation (7) in paper.[33] Consequently, even a small deviation in the frequency and mode shape values might lead to failed tracking. This challenge underscores the need for setting the allowed minimum eigenvalue, $\lambda_{\min_j}$, in Equation (12).

Taking into account a special circumstance in this numerical example, where the frequency and mode shape values of mode 1 markedly differ from the other modes, and considering that mode 1 can be explicitly discerned using the MPE method, a workaround for the simple tracking algorithm could be achieved by setting a larger threshold specifically for mode 1. However, a more complex situation arises with mode 8, where it is not always accurately identified, and some spurious modes resembling mode 8 are recognized by the MPE method. This scenario may occur when the external load is insufficient to properly excite this mode or when the modal damping is comparatively high. Figure 7 shows that the algorithm based on reference modes misinterpreted mode 8 as mode 7 after several datasets. Table 1 explains this occurrence: The variability of the mode shape values across the initial

nine datasets caused the threshold of the simple tracking algorithm to increase. And given the closeness of the frequencies of modes 7 and 8, the spurious modes in datasets 10–13 were iteratively tracked, culminating in the misinterpretation of mode 7 in dataset 14 as mode 8. In contrast to mode 1, setting a smaller threshold specifically for mode 8 could result in missed tracking of potential physical modes, leading to a reduced modal tracking rate (MTR). Moreover, such misclassification could still occur even with a lower threshold. This is because any misidentified spurious mode will be taken as the reference mode for the subsequent dataset, potentially leading to another misidentification. Once one mode such as mode 8 is mistakenly tracked as the easier-to-track one, such as mode 7, the tracking cannot be recorrected. Such low fault tolerance contributes to poor performance in this complex scenario. On the other hand, the proposed algorithm incorporates the modal probability model $(N_{l+1}(\boldsymbol{\mu}_j, \boldsymbol{\Sigma}_j))$ derived from multiple previous datasets. As it also encapsulates the historical information of the mode, it is less prone to the influence of isolated spurious modes.

MTR and some statistical characteristics (mean, variance) of the modal parameter distance between the tracked mode and analytical mode are listed in Table 2. The MTR is calculated by dividing the number of tracked modes by the number of datasets (300). f_{mean} is the mean of the natural frequency difference between the tracked modes and the analytical modes. The other symbols are similar. Since it is difficult to graphically display the change in each mode shape over time, Table 2 provides the statistics of the modal assurance
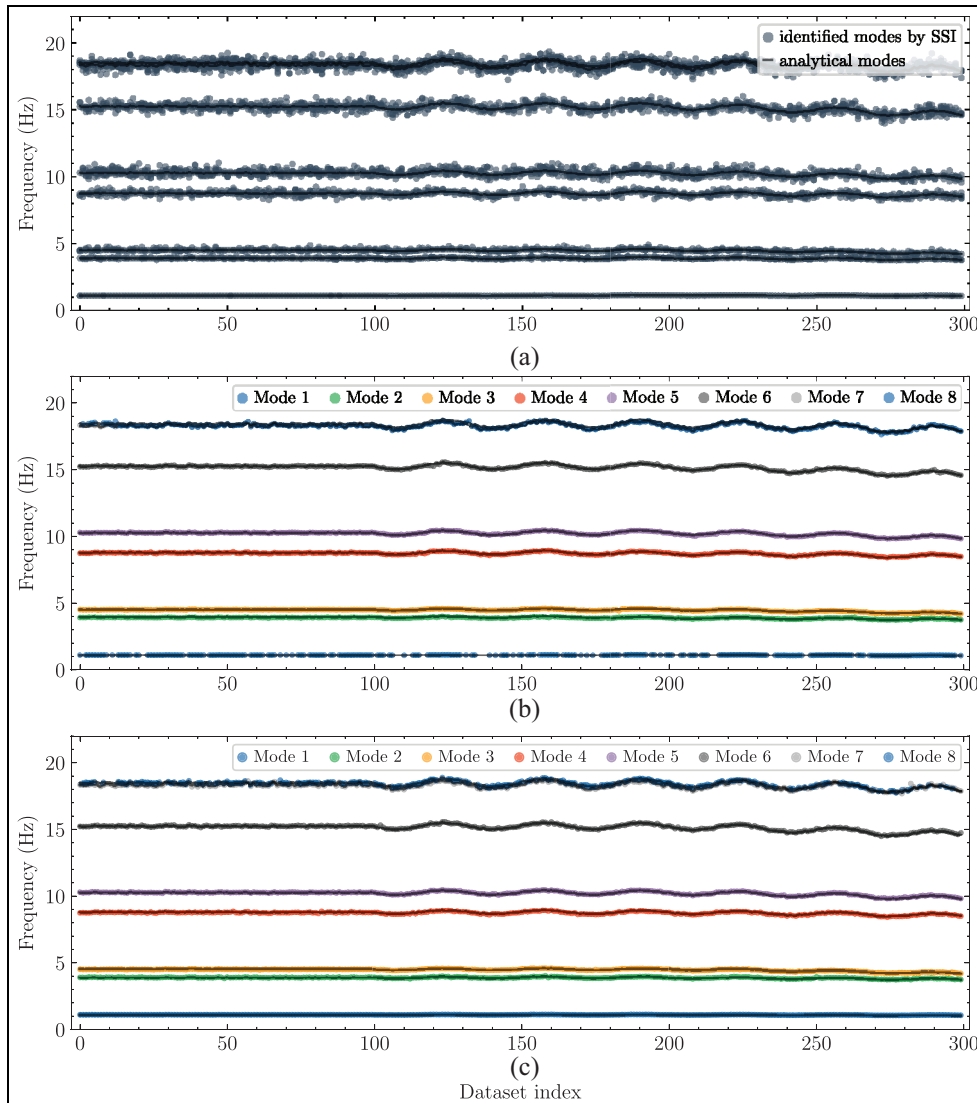
Figure 7. Modal tracking for the numerical example by: (a) SSI only, (b) the simple modal tracking algorithm, and (c) the proposed algorithm.

criterion (MAC)[34] between the tracked mode shapes and the analytical mode shapes. As the mode shapes approach each other, the MAC tends to 1. The relatively low MTR for mode 1 and the low MAC_{mean} for the reference-based algorithm correspond with the depiction in Figure 7.

Figure 8 shows the tracking of the damping ratios. The modal damping ratio of each mode has a large dispersion and is distinguishable. This is consistent with what is described in Section "Obtain physical modes using Bayesian inference." In addition, it is related to the vibration energy of a real-world structure. The considerable uncertainty of the modal damping ratio makes it difficult to reflect the algorithm's performance, so it will not be mentioned again.

Empirical studies

In this section, a real-world civil structure (the Z24 bridge) is used to illustrate the algorithm. The Z24 bridge was located in the canton of Bern near Solothurn, Switzerland. It was part of a road connection between the villages of Koppigen and Utzenstorf, overpassing the A1 highway between Bern and Zürich. It was a classical posttensioned concrete two-cell box-girder bridge with a main span of 30 m and two side spans of 14 m (Figure 9). The modal parameters of the Z24 bridge are shown in Figure 10. The bridge, which dated from 1963, was demolished at the end of 1998 because a new railway adjacent to the highway required a new bridge with a larger side span. More

Table 1. Modal tracking results of the two algorithms for the first 14 datasets.

index	1	2	3	4	5	6	7	8	9	10	11	12	13	14
φ_8	—	0.49	—	0.37	0.21	0.41	—	—	0.48	0.17	−0.01	−0.03	0.01	−0.27
	—	—0.62	—	−0.71	−0.76	−0.65	—	—	−0.59	−0.73	−0.73	−0.70	−0.62	−0.56
	—	0.45	—	0.32	0.25	0.40	—	—	0.49	0.24	0.03	−0.13	−0.25	−0.30
	—	−0.27	—	−0.36	−0.39	−0.32	—	—	−0.24	−0.41	−0.43	−0.34	−0.25	−0.40
	—	0.09	—	−0.11	−0.13	0.13	—	—	0.10	−0.14	−0.32	−0.35	−0.53	−0.47
	—	−0.31	—	−0.35	−0.40	−0.35	—	—	−0.34	−0.44	−0.42	−0.51	−0.46	−0.38
f_{n_8}	—	18.46	—	18.49	18.52	18.56	—	—	18.52	18.51	18.53	18.33	18.65	18.35
φ_8	—	0.49	0.20	0.37	0.21	0.41	—	—	0.48	—	—	—	—	0.41
	—	−0.62	−0.74	−0.71	−0.76	−0.65	—	—	−0.59	—	—	—	—	−0.65
	—	0.45	0.22	0.32	0.25	0.40	—	—	0.49	—	—	—	—	0.42
	—	−0.27	−0.40	−0.36	−0.39	−0.32	—	—	−0.24	—	—	—	—	−0.32
	—	0.09	−0.16	−0.11	−0.13	0.13	—	—	0.10	—	—	—	—	0.06
	—	−0.31	−0.42	−0.35	−0.40	−0.35	—	—	−0.34	—	—	—	—	−0.35
f_{n_8}	—	18.46	18.53	18.49	18.52	18.56	—	—	18.52	—	—	—	—	18.57

The upper section displays the results obtained from the algorithm based on reference modes, while the lower section showcases the results obtained from the proposed algorithm. The mode shape and frequency of mode 8 is represented by φ_8 and f_n. For clear representation, all mode shape vectors are normalized to have a sum of squares equal to 1, that is, $\varphi_8^T \varphi_8 = 1$. The "—" symbol indicates that the corresponding modal tracking method did not identify any potential modes for mode 8.

Table 2. Modal tracking rate and statistical characteristics for the numerical example.

Mode	1	2	3	4	5	6	7	8
MTR	0.7933	1.0000	1.0000	1.0000	1.0000	1.0000	0.9967	0.9867
f_{mean}	0.0003	−0.0001	0.0005	0.0036	−0.0007	−0.0036	0.0026	−0.1403
f_{var}	0.0027	0.0122	0.0105	0.0190	0.0185	0.0314	0.0434	0.0783
MAC_{mean}	0.9856	0.9932	0.9971	0.9986	0.9993	0.9991	0.9786	0.2500
MAC_{var}	0.0334	0.0101	0.0041	0.0020	0.0011	0.0011	0.1056	0.2614
MTR	1.0000	1.0000	1.0000	1.0000	1.0000	1.0000	0.9967	0.7200
f_{mean}	0.0002	−0.0001	0.0016	0.0034	−0.0001	0.0000	0.0026	−0.0055
f_{var}	0.0026	0.0133	0.0094	0.0188	0.0171	0.0309	0.0446	0.0286
MAC_{mean}	0.9662	0.9938	0.9975	0.9988	0.9994	0.9993	0.9797	0.9161
MAC_{var}	0.0563	0.0097	0.0034	0.0016	0.0007	0.0007	0.1026	0.1359

MAC: modal assurance criterion; MTR: modal tracking rate.
The upper section displays the indices obtained from the algorithm based on reference modes, while the lower section showcases the indices obtained from the proposed algorithm.
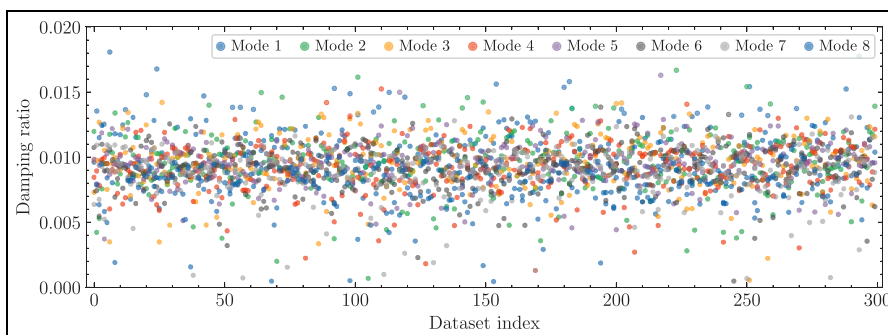

Figure 8. Damping ratio tracking for the numerical example.

information about the Z24 bridge can be found in researches.[35,36]

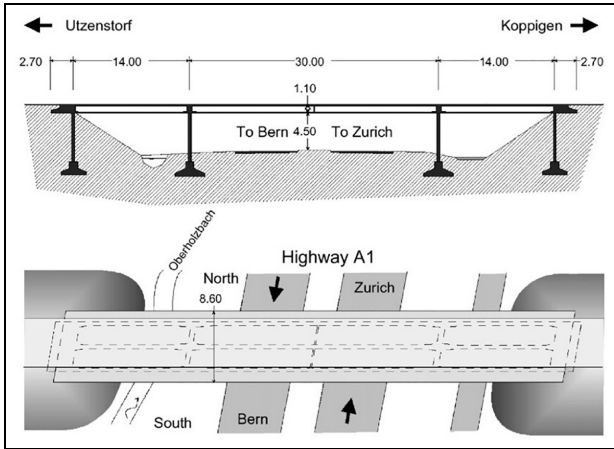A long-term continuous monitoring test was performed on the Z24 bridge 1 year before demolition. In

Figure 9. Front view and top view of the Z24 bridge.[35]

the month before its complete demolition, the bridge gradually suffered controlled damage while the

continuous monitoring system was still in operation. The Z24 long-term monitoring and short-term progressive damage test data have served as benchmark data in numerous scientific studies.[10,33,37–43]

Sixteen accelerations were measured on the bridge at different points and in different directions to monitor the bridge dynamics. Each hour, 65,536 acceleration samples, taken from the 16 sensors, were collected as one response set. Although the accelerometers were specially designed for long-term use, some sensors failed or were damaged. In this section, five effective lateral and vertical sensors were selected. After excluding some exception datasets, 5599 response sets from November 10, 1997, to September 10, 1998, were obtained.

Figure 11 displays the stabilization diagram of a response set for the Z24 bridge. It shows both clearly defined vertical lines as well as "crowded" lines that may represent spurious modes. Furthermore, physical
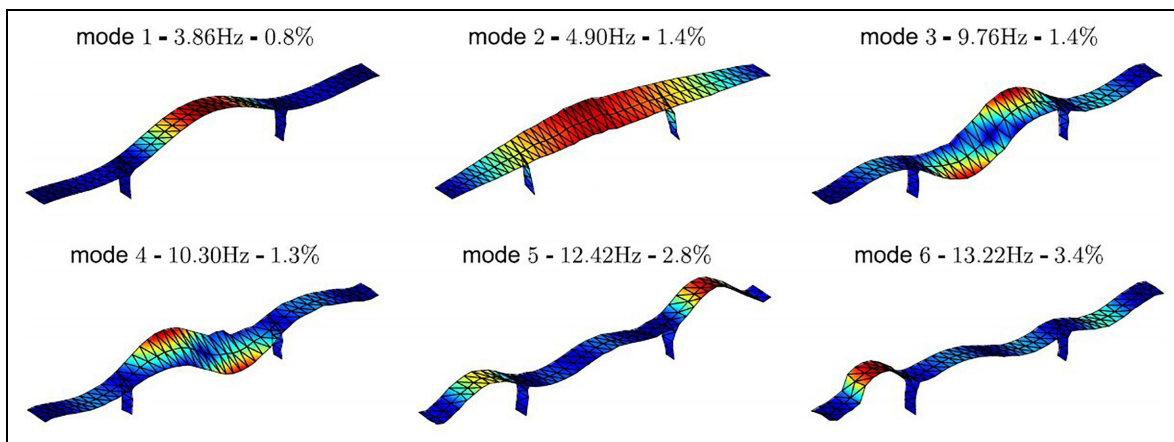

Figure 10. Natural frequencies, damping ratios, and mode shapes of the Z24 bridge for damage scenario 8.[10]
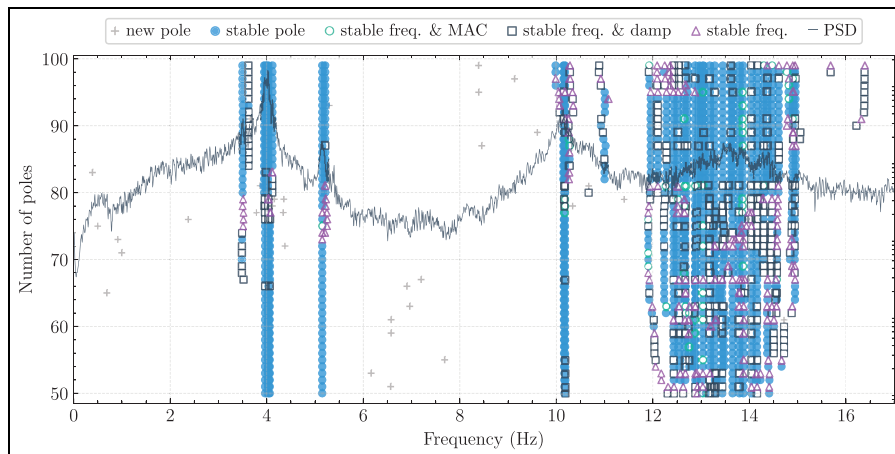

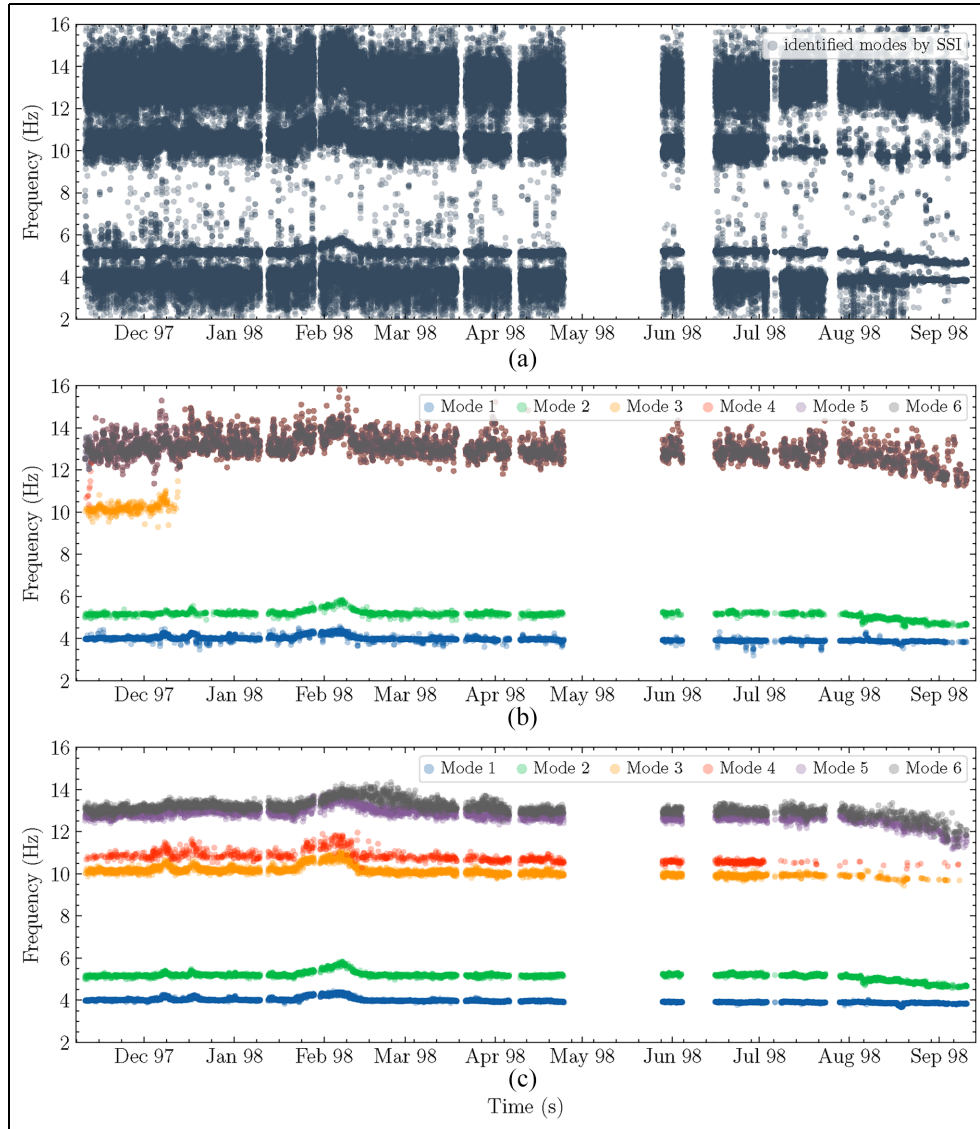**Figure 11.** Stabilization diagram for the Z24 bridge (Time: November 13, 1997, 02:00 pm).

Figure 12. Modal tracking for the Z24 bridge by: (a) stochastic subspace identification (SSI) only, (b) the simple modal tracking algorithm, and (c) the proposed algorithm.

mode 3 (as shown in Figure 10) is not identified in this response set, making it more challenging to track modes continuously. In Figure 12(a), the results obtained by applying the MPE method iteratively for modal tracking on 5599 response sets are presented. This figure illustrates that the frequencies of modes identified by SSI even cover the frequencies of two physical modes, such as modes 3 and 4, as well as modes 5 and 6. This further complicates the task of modal tracking.

The proposed tracking algorithm employed the following hyperparameters: a minimum allowed eigenvalue of 0.001 times the frequency of mode j, a percentile value of 98% for the Gaussian distribution, and the last 50 (m) successfully identified modes are utilized to

obtain $\boldsymbol{\mu}_j$ and $\boldsymbol{\Sigma}_j$. Six clusters were selected for the six physical modes depicted in Figure 10, with the frequencies (4.01, 5.16, 10.14, 10.83, 12.77, 13.07).

Figure 12(b) and (c) shows the modal tracking results obtained by the simple algorithm and proposed algorithm, respectively. Regretfully, since it is impossible to obtain the analytical solution of the modal parameters of Z24 bridge corresponding to each response set, the table similar to tables in Section "Numerical example" cannot be given here. Other studies[33,36,41] also tracked the modal parameters of the Z24 bridge manually or automatically. However, they typically only tracked up to four modes continuously, and did not provide information on which mode is being tracked.

Figure 12(b) and (c) demonstrate that the proposed algorithm can effectively track a complex case, whereas the simple algorithm fails to track modes 3–6, and there are also outliers for modes 1 and 2. Taking mode 4 as an example, in cases where it was not identified by SSI (as shown in Figure 11), the simple algorithm may incorrectly identify a spurious mode (if it exists) as mode 4. This misidentification of mode 4 can then lead to further misidentifications in subsequent response sets. Due to the relatively close modal parameters of modes 4 and 5, mode 4 was ultimately tracked as mode 5 after several spurious modes were tracked. The tracking of mode 3 exhibited similar behavior to that of mode 4. Similar to mode 8 in the numerical example, setting small thresholds specifically for mode 3 or mode 4 can prevent such misclassifications. However, this might result in much fewer potential physical modes being tracked, particularly during the period around February 1998, than there should have been. On the contrary, the proposed algorithm can hardly identify a spurious mode as mode 4. And even if spurious modes are identified, they are unlikely to affect the modal tracking of the subsequent response set. This is because the algorithm takes into account the historical modal parameters from recent response sets, which inform the algorithm about the characteristics of mode 4 in the past.

For the period around February 1998, there was a temporary but significant frequency increase and recovery. This was related to a change in the asphalt layer during a freezing period, which contributed significantly to the stiffness of the bridge. Peeters et al.[40] demonstrated the bilinear behavior of natural frequencies at temperatures below and above the freezing point. In addition, progressive damage tests were performed on the Z24 bridge after August 1998. Figure 12(c) shows that the frequencies decreased significantly during that period. The strategy that only considers the modal probability model from multiple previous response sets may fail when such significant changes in modal parameters happen. However, our algorithm can still perform well since it also considers the modes identified from the most recent response set, improving the probability density in Equation (2).

Conclusions

This paper presents an algorithm for long-term continuous and automatic modal tracking. The algorithm determines the physical modes from the results of existing MPE methods through Bayesian inference. It performs well even in situations where the modal parameters undergo significant changes, and despite the presence of numerous spurious modes.

Two kinds of information are considered in the Bayesian inference model. They are (1) modes identified from the most recent response set, which are also the reference modes, and (2) the modal probability model from multiple previous response sets. These two considerations interact to help better select the physical modes from the MPE. Whenever a physical mode is identified, it is used for the update of the two kinds of information. The update makes Bayesian inference always run on the latest prior knowledge.

The algorithm was applied to a numerical example and a real-world civil structure, the Z24 bridge. A simple modal tracking algorithm was used for comparison. The results indicate that for straightforward cases such as modes 2 through 7 in the numerical example, both algorithms demonstrate solid performance. Nevertheless, in more complex scenarios, like modes 1 and 8 in the numerical example or modes 3 and 4 of the Z24 bridge, the proposed algorithm proves superior to the simple modal tracking algorithm. Furthermore, compared to other studies that have tracked modal parameters of the Z24 bridge, the proposed algorithm was able to track more modes, that is, modes 5 and 6, and accurately classified all modes.

The main time-consuming part of the algorithm lies in SSI-COV. Bayesian inference is fast due to the small amount of data involved and all the analytical equations. It took about 60 s with M1-chip Macbook Air to apply the Bayesian inference in the algorithm to all the modes obtained by MPE from the 5599 response sets of the Z24 Bridge.

The algorithm also has some limitations. Given the adaptive nature of the algorithm, which uses data from previous datasets, the algorithm will produce good results for applications on structures subjected to operational/environmental conditions varying under a continuous function. However, it will perform badly if there are sudden large changes in the modal parameters. There will be no way to deal with such sudden and dramatic changes when they occur frequently. But if the mutation is rare, one could reinitialize the algorithm hyperparameters and run the algorithm again. In addition, since the algorithm determines the physical modes from the MPE results, the performance upper limit of the algorithm depends on the MPE method adopted. However, from another point of view, a better MPE method also produces better algorithm performance.

Declaration of conflicting interests

ORCID iDs

Siyuan Sun ⒾⒹ https://orcid.org/0000-0002-6707-3242
Haitao Zhu ⒾⒹ https://orcid.org/0000-0003-0698-6897

References

1. Charbonnel PÉ. Fuzzy-driven strategy for fully automated modal analysis: Application to the SMART2013 shaking-table test campaign. *Mech Syst Signal Process* 2021; 152: 107388.
2. Ubertini F, Comanducci G, Cavalagli N, et al. Environmental effects on natural frequencies of the San Pietro bell tower in Perugia, Italy, and their removal for structural performance assessment. *Mech Syst Signal Process* 2017; 82: 307–322.
3. Neu E, Janser F, Khatibi AA, et al. Fully Automated operational modal analysis using multi-stage clustering. *Mech Syst Signal Process* 2017; 84: 308–323.
4. Cardoso R, Cury A and Barbosa F. A robust methodology for modal parameters estimation applied to SHM. *Mech Syst Signal Process* 2017; 95: 24–41.
5. Rainieri C and Fabbrocino G. Development and validation of an automated operational modal analysis algorithm for vibration-based monitoring and tensile load estimation. *Mech Syst Signal Process* 2015; 60–61: 512–534.
6. Ubertini F, Gentile C and Materazzi AL. Automated modal identification in operational conditions and its application to bridges. *Eng Struct* 2013; 46: 264–278.
7. Au S-K, Brownjohn JMW, Li B, et al. Understanding and managing identification uncertainty of close modes in operational modal analysis. *Mech Syst Signal Process* 2021; 147: 107018.
8. Hou R, Wang X, Xia Q, et al. Sparse Bayesian learning for structural damage detection under varying temperature conditions. *Mech Syst Signal Process* 2020; 145: 106965.
9. Tronci E, De Angelis M, Betti R, et al. Multi-stage semi-automated methodology for modal parameters estimation adopting parametric system identification algorithms. *Mech Syst Signal Process* 2022; 165: 108317.
10. Reynders E, Houbrechts J and De Roeck G. Fully automated (operational) modal analysis. *Mech Syst Signal Process* 2012; 29: 228–250.
11. Peeters B and Roeck GD. Reference-based stochastic subspace identification for output-only modal analysis. *Mech Syst Signal Process* 1999; 13(6): 855–878.
12. Magalhães F, CunhaÁ and Caetano E. Online automatic identification of the modal parameters of a long span arch bridge. *Mech Syst Signal Process* 2009; 23(2): 316–329.
13. Tronci EM, De Angelis M, Betti R, et al. Semi-automated operational modal analysis methodology to optimize modal parameter estimation. *J Optimiz Theor Appl* 2020; 187(3): 842–854.
14. Wang X, Zhu Z and Au SK. Bayesian operational modal analysis of structures with tuned mass damper. *Mech Syst Signal Process* 2023; 182: 109511.
15. Zhang FL, Kim CW and Goi Y. Efficient Bayesian FFT method for damage detection using ambient vibration data with consideration of uncertainty. *Struct Contr Health Monitor* 2021; 28(2): e2659.
16. Zhang F-L and Ni Y-C. Operational modal analysis of super tall buildings by a Bayesian approach. In Rivas-Lopez M, Fuentes WF and Sergiyenko O (eds.) *Structural health monitoring-measurement methods and practical applications.* Croatia: InTech, 2017.
17. Au SK. *Operational modal analysis.* Singapore: Springer Singapore, 2017.
18. Au SK. Fast Bayesian ambient modal identification in the frequency domain, Part II: Posterior uncertainty. *Mech Syst Signal Process* 2012; 26: 76–90.
19. Au SK. Fast Bayesian ambient modal identification in the frequency domain, Part I: Posterior most probable value. *Mech Syst Signal Process* 2012; 26: 60–75.
20. Huang TL and Chen HP. Mode identifiability of a cable-stayed bridge using modal contribution index. *Smart Structures & Systems* 2017; 20(2): 115–126.
21. Zhou K, Zhang JW and Li QS. Control performance of active tuned mass damper for mitigating wind-induced vibrations of a 600-m-tall skyscraper. *J Build Eng* 2022; 45: 103646.
22. Zhou K and Li QS. Vibration mitigation performance of active tuned mass damper in a super high-rise building during multiple tropical storms. *Eng Struct* 2022; 269: 114840.
23. Zhang Q, Luo X, Ding J, et al. Dynamic response evaluation on TMD and main tower of Shanghai Tower subjected to Typhoon In-Fa. *Struct Des Tall Special Build* 2022; 31(9): e1929.
24. He YC and Li Q. Dynamic responses of a 492-m-high tall building with active tuned mass damping system during a typhoon: DYNAMIC RESPONSES OF A TALL BUILDING WITH ATMD SYSTEM. *Struct Contr Health Monitor* 2013; 21(5): 705–720.
25. Yang B, Pan L, Zhu H, et al. Spatiotemporal correlation analysis of the dynamic response of supertall buildings under ambient wind conditions. *Struct Des Tall Special Build* 2022; 31(4): e1914.
26. Yang X-M, Yi T-H, Qu C-X, et al. Continuous tracking of bridge modal parameters based on subspace correlations. *Struct Contr Health Monitor* 2020; 27(10): e2615.
27. Cabboi A, Magalhães F, Gentile C, et al. Automated modal identification and tracking: Application to an iron arch bridge: Automated Modal Identification and Tracking. *Struct Contr Health Monitor* 2017; 24(1): e1854.
28. Mao JX, Wang H and Spencer JBF. Gaussian mixture model for automated tracking of modal parameters of long-span bridge. *Smart Struct Syst* 2019; 24(2): 243–256.
29. Tronci E, De Angelis M, Betti R, et al. Vibration-based structural health monitoring of a RC-masonry tower

equipped with non-conventional TMD. *Eng Struct* 2020; 224: 111212.

30. Tronci EM. *Damage sensitive features. from classic parameters to new indicators*. Phdtronci 2019 damage,, Ph. D. dissertation, Sapienza University of Rome, 2019.

31. Peeters B. *System identification and damage detection in civil engineering*. University of Oxford, 2000.

32. Slotani M. Tolerance regions for a multivariate normal population. *Ann Inst Statist Math* 1964; 16(1): 135–153.

33. Langone R, Reynders E, Mehrkanoon S, et al. Automated structural health monitoring based on adaptive kernel spectral clustering. *Mech Syst Signal Process* 2017; 90: 64–78.

34. Kim TS and Kim YY. Mac-based mode-tracking in structural topology optimization. *Comput Struct* 2000; 74(3): 375–383.

35. Maeck J and De Roeck G. Description of Z24 benchmark. *Mech Syst Signal Process* 2003; 17(1): 127–131.

36. Reynders E and De Roeck G. Vibration-based damage identification: The Z24 bridge benchmark. In Beer M, Kougioumtzoglou IA, Patelli E, et al. (eds.) *Encyclopedia of earthquake engineering*. Berlin, Heidelberg: Springer Berlin Heidelberg, 2014, pp. 1–8.

37. Maeck J, Peeters B and De Roeck G. Damage identification on the Z24 bridge using vibration monitoring. *Smart Mater Struct* 2001; 10(3): 512–517.

38. Teughels A and De Roeck G. Structural damage identification of the highway bridge Z24 by FE model updating. *J Sound Vibr* 2004; 278(3): 589–610.

39. Reynders E and De Roeck G. A local flexibility method for vibration-based damage localization and quantification. *Journal of Sound and Vibration* 2010; 329(12): 2367–2383.

40. Peeters B and De Roeck G. One-year monitoring of the Z24-Bridge: Environmental effects versus damage events. *Earthq Eng Struct Dyn* 2001; 30(2): 149–171.

41. Reynders E, Wursten G and De Roeck G. Output-only structural health monitoring in changing environmental conditions by means of nonlinear system identification. *Struct Health Monitor* 2014; 13(1): 82–93.

42. Peeters B and Ventura CE. Comparative study of modal analysis techniques for bridge dynamic characteristics. *Mech Syst Signal Process* 2003; 17(5): 965–988.

43. Reynders E and De Roeck G. Reference-based combined deterministic–stochastic subspace identification for experimental and operational modal analysis. *Mech Syst Signal Process* 2008; 22(3): 617–637.